

# Towards Minimal Fine-Tuning of VLMs

Tiange Luo<sup>1,2</sup> Lajanugen Logeswaran<sup>2</sup> Jaekyeom Kim<sup>2</sup> Justin Johnson<sup>1,†</sup> Honglak Lee<sup>1,2,†</sup>  
 University of Michigan<sup>1</sup> LG AI Research<sup>2</sup> <sup>†</sup> equal advising

## Abstract

We introduce *Image-LoRA*, a lightweight parameter efficient fine-tuning (PEFT) recipe for transformer-based vision-language models (VLMs). *Image-LoRA* applies low-rank adaptation only to the value path of attention layers within the visual-token span, reducing adapter-only training FLOPs roughly in proportion to the visual-token fraction. We further adapt only a subset of attention heads, selected using head influence scores estimated with a rank-1 *Image-LoRA*, and stabilize per-layer updates via selection-size normalization. Across screen-centric grounding and referring benchmarks spanning text-heavy to image-heavy regimes, *Image-LoRA* matches or closely approaches standard LoRA accuracy while using fewer trainable parameters and lower adapter-only training FLOPs. The method also preserves the pure-text reasoning performance of VLMs before and after fine-tuning, as further shown on *GSM8K*.

## 1. Introduction

Low-rank adaptation (LoRA) [9] has become a strong baseline for post-training of large language models because it exposes a small, trainable subspace while keeping the base network frozen [18]. However, parameter-efficient tuning (PEFT) for transformer-based vision-language models (VLMs) presents different constraints than text-only LLMs: prompts often contain long stretches of text mixed with images, and attention modules comprise many heads, even though only a subset appears to carry most of the routing signal for visual reasoning, such as grounding and pointing [1, 11]. Existing PEFT recipes typically treat all tokens and all heads uniformly, which leaves efficiency on the table. We revisit LoRA through the lens of VLM structure and ask: what if we only adapt the parts that directly affect grounded vision-text reasoning?

Our first design choice is visual-token only fine-tuning. Restricting adaptation to the visual-token span reduces adapter-only training FLOPs roughly in proportion to the visual-token fraction, as it avoids computation through both the input prompt and the output text. A further benefit is

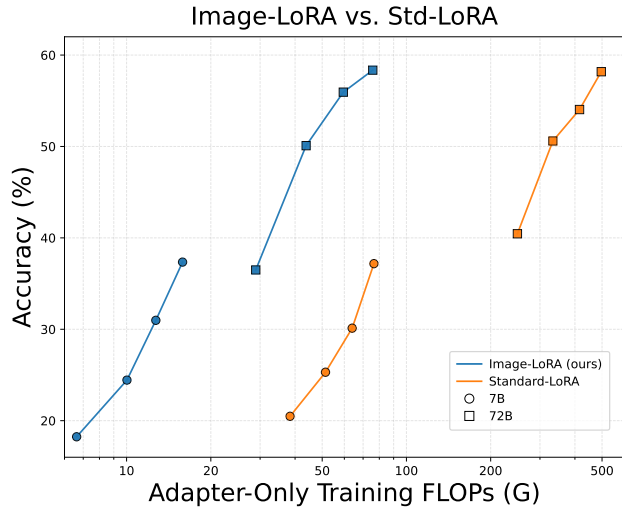


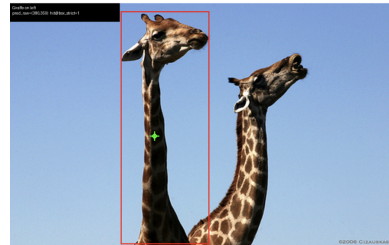
Figure 1. **Image-LoRA vs. Standard LoRA.** Comparison of accuracy and adapter-only training FLOPs on ScreenSpot-Pro. Points are connected across increasing input-text:image token ratios (1:2 → 1:5), where we control the ratios by dynamically adjusting image sizes. FLOPs are token-limited and computed as forward + backward multiply-adds.

that fine-tuning only on the visual-token span ensures that the adapted weights never affect the pure-text reasoning performance of the fine-tuned VLMs, as also demonstrated in our *GSM8K* [5] experiment. This design is further supported by recent evidence that textual information can be routed through visual-token channels [4, 24], suggesting that adapting visual tokens alone could be powerful. To ensure that updating the attention paths on the visual-token span meaningfully influences the representations of text tokens, we compared adapting  $K$  and  $V$  and found that adapting only  $V$  performs best. Additionally, localization-style objectives (e.g., pointing) place supervision primarily in the pixels, while the long text prompt mainly serves as task scaffolding. Concentrating adapters on the visual span allocates capacity where the loss is informative and may discourage shortcircuiting through language priors, as shown in our *ViLP* [15] experiment.

Second, rather than treating all attention heads equally,



ScreenSpot-Pro (target bbox in green)



RefCOCO (target bbox in red)

**Q:** Betty is saving money for a new wallet which costs \$100. Betty has only half of the money she needs. Her parents decided to give her \$15 for that purpose, and her grandparents twice as much as her parents. How much more money does Betty need to buy the wallet?

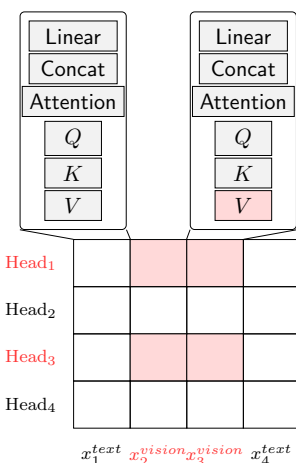
**A:** 5

GSM8K



ViLP

**Q:** Who is painting the Mona Lisa in the image?  
**A:** Vincent Van Gogh



Adapting on selected heads & vision token spans & value path solely

Image-LoRA

Figure 2. **Overview. Left:** We evaluate Image-LoRA on grounded vision–language reasoning datasets, including ScreenSpot-Pro [14] and RefCOCO [12], where the model takes a text query with its system prompt and outputs a point indicating the referred object. We further evaluate on the pure text reasoning dataset GSM8K [5] to confirm that Image-LoRA does not affect pure text reasoning, and on ViLP [15] containing VQAs both aligned with and against language priors to show that Image-LoRA may mitigate shortcutting through such priors. **Right:** Image-LoRA is applied only to selected heads along the value path of attention layers within the visual-token span (the pink area).

we ask whether a small set suffices for our tasks. A naïve approach is a finite-difference ablation: enable one head at a time, recompute the loss over the dataset, and keep the heads with the largest loss drops—but this is prohibitively expensive. To this end, we propose a head influence score estimated by attaching a rank-1 Image-LoRA to every head, running a single forward–backward pass with the task loss, and scoring each head by the squared gradient norm of its Image-LoRA parameters – a first-order empirical-Fisher proxy that identifies a high-impact subset without iterative search. After head selection, different layers may retain different numbers of heads—unlike standard LoRA, which updates all heads per layer. To maintain stable per-layer update magnitude, we apply a selection-size layer normalization as part of Image-LoRA.

Putting these pieces together, we propose *Image-LoRA*. The adapter is injected pre-RoPE (rotary position embeddings) and pre-KV-cache so that its effect persists into decoding. Proof-of-concept experiments on screen-centric grounding and referring expression datasets (ScreenSpot-Pro [14] and RefCOCO [12]) span a wide range of input-text:image token ratios (1:1/2, 1:1, 1:2, 1:3, 1:4, 1:5) along with QWen2.5-VL-7B, QWen2.5-VL-72B, and LLaVA-NeXT-7B models. We enforce the chosen ratio during both training and evaluation to probe regimes

from text-heavy to image-heavy. Our results, shown in Figure 1, demonstrate that Image-LoRA retains accuracy while reducing trainable parameters and adapater-only training FLOPs, especially in image-heavy settings. Furthermore, experiments on GSM8K [5] show that Image-LoRA preserves pure-text reasoning performance, whereas standard LoRA may not. We also evaluate on ViLP [15], a VQA dataset deliberately constructed to follow or break language priors, where Image-LoRA outperforms standard LoRA. In the ablation studies, we further evaluate the proposed head-selection method against correlation-based, global-random, and per-layer-random baselines, as well as examine various design choices for Image-LoRA.

Although our proof-of-concept experiments above show some promising signals for Image-LoRA, our experimental scale is limited, and fundamental constraints inherent to the Image-LoRA formulation remain and require further investigation, as discussed in Section 5.

Collectively, we present a vision-orientated PEFT recipe for transformer-based VLMs. By restricting adaptation to the visual-token span, stabilizing updates when adapting a subset of attention heads, and preserving pure-text reasoning behavior, Image-LoRA offers a structured step toward enabling web-scale vision pre-training on top of existing reasoning LLMs [10].

## 2. Related Works

**PEFT of VLMs.** A common approach to efficient fine-tuning of VLMs is to reduce the number of parameters to update, which is often called parameter-efficient fine-tuning (PEFT). One important milestone in PEFT is leveraging the reparameterization of the parameters of models, often notably represented by low-rank adaptation (LoRA) [9], which has also been shown to be effective for VLMs [7, 21, 27, 32]. Recently, Schulman et al. [18] examined the effects of applying LoRA either only to attention layers or to all layers, including MLP/MoE layers, a topic explored in prior works [6, 8, 20, 23, 26, 31]. In contrast, our work explores a more structured approach—applying LoRA selectively to attention heads and to the visual token span only. Meanwhile, Shuttleworth et al. [19] reported findings that contradict [18], showing that LoRA can behave differently from full fine-tuning, with both studies focusing on pure text-based benchmarks. In contrast, we focus on visual reasoning tasks, including both grounding and VQA tasks.

**Token selection and reduction for VLMs.** Token selection and reduction have been applied to improve VLM inference efficiency. Token pruning removes unimportant input tokens based on relevance criteria. FastV [3] ranks visual tokens by attention scores, while SparseVLM [30] first filters relevant text tokens and then keeps the most attended visual tokens. Token merging instead combines similar tokens to reduce sequence length. PuMer [2] prunes low-saliency visual tokens and merges similar tokens within the same modality, and VisionZip [25] merges non-dominant visual tokens based on attention scores. On the other hand, we explore a different angle through token selection—investigating how constraining the set of input tokens can make the fine-tuning of VLMs (rather than inference) more efficient by applying Image-LoRA to the visual-token span only. This offers two benefits: (1) it saves FLOPs from both input and output text, and (2) such LoRA fine-tuning does not alter the pure-text reasoning behavior of VLMs.

**Attention head selection for VLMs.** Prior work shows that attention heads in LLMs and VLMs differ in their task importance. Michel et al. [17] demonstrate redundancy among heads in language models and prune them by measuring loss sensitivity to head masking, while [22, 29] similarly assess head importance via backpropagated gradients and achieve comparable performance after pruning. Furthermore, Khaki et al. [13] accelerate LLM fine-tuning with an SVD-based sparsity estimator over the model’s pre-trained weight matrix. Kang et al. [11] identify “localization heads” crucial for visual grounding and leverage their attention maps at inference, and Zhang et al. [28] enhance perception by using the most attentive layer for test-time

visual cropping. This paper develops an efficient first-order approximation for head selection as a simple complement to our proposed Image-LoRA, and shows that, when combined with the proposed layer-wise head-selection size normalization, our method performs well even with irregularly selected attention heads.

## 3. Method

We propose a parameter-efficient fine-tuning recipe for steering transformer-based VLMs on visual reasoning tasks while minimizing trainable parameters and adapter-only FLOPs, while preserving the pure-text reasoning ability of the VLM. We focus on tasks where visual reasoning is the dominant component (e.g., text-conditioned visual localization) and leave extensions to other task types for future work.

Our approach achieves *minimal* adaptation through three forms of selectivity: 1. **Token selectivity (visual-only):** We adapt representations only for visual tokens, rather than for all tokens (including text). This contrasts with standard PEFT approaches (e.g., LoRA) that introduce adapters in projections shared by every token. 2. **Head selectivity (subset of attention heads):** We update only a subset of attention heads and introduce a selection procedure to identify a diverse, salient set of heads relevant to visual reasoning. 3. **Projection selectivity (value-only):** In contrast to LoRA, which typically inserts low-rank adapters into the query ( $Q$ ), key ( $K$ ), value ( $V$ ), and output ( $O$ ) projections, we attach adapters only to the value ( $V$ ) projections of the selected heads and only for visual tokens.

### 3.1. Background

**Transformer Multi-Head Attention.** For a sequence of length  $T$ , let the input and output of a transformer layer be  $X, Y \in \mathbb{R}^{T \times d_{\text{hidden}}}$ , where  $d_{\text{hidden}}$  is the model width. Multi-head attention can be written as

$$Y = \text{MultiHead}(X) = \text{Concat}(O^{(1)}, \dots, O^{(H)}) W_O$$

$$\text{where } O^{(h)} = \text{softmax} \left( \frac{Q^{(h)} K^{(h)\top}}{\sqrt{d_k}} + \text{Mask} \right) V^{(h)},$$

$$Q^{(h)} = X W_Q^{(h)}, \quad K^{(h)} = X W_K^{(h)}, \quad V^{(h)} = X W_V^{(h)}.$$

Here  $H$  is the number of attention heads.  $\text{Mask} \in \mathbb{R}^{T \times T}$  is the causal mask with  $\text{Mask}_{ij} = 0$  if  $j \leq i$  and  $\text{Mask}_{ij} = -\infty$  otherwise; the softmax is applied row-wise. The query and key dimension and value dimension are denoted by  $d_k$  and  $d_v$ , respectively (for simplicity, we assume  $d_k = d_v = d_{\text{hidden}}/H = d_{\text{head}}$ ), and the learnable projection matrices are  $W_{\{Q, K, V\}}^{(h)} \in \mathbb{R}^{d_{\text{hidden}} \times d_{\text{head}}}$ ,  $W_O \in \mathbb{R}^{(H \times d_{\text{head}}) \times d_{\text{hidden}}}$ .

**LoRA.** LoRA is a parameter-efficient fine-tuning method that models updates to weight matrices as low-rank adaptations. LoRA represents a linear map such as  $V = XW_V$  (superscript  $(h)$  avoided for brevity) as a low-rank decomposition with  $r \ll \min(d_{\text{head}}, d_{\text{hidden}})$ ,

$$\Delta W_V = AB, \quad A \in \mathbb{R}^{d_{\text{hidden}} \times r}, \quad B \in \mathbb{R}^{r \times d_{\text{head}}},$$

yielding the modified forward pass

$$V = X(W_V + \Delta W_V) = XW_V + XAB \cdot s, \quad s = \frac{\alpha}{r} \gamma,$$

where  $\alpha$  is a scaling hyperparameter,  $\gamma$  is a learned scalar gate, and  $r$  is the adaptation rank. The original weight  $W_V$  is frozen; only  $(A, B, \gamma)$  are trained.

### 3.2. Image-LoRA

**Vision Tokens Only.** The first distinguishing property of our method is that we only learn to update representations corresponding to vision tokens, unlike the standard LoRA which treats both vision and text tokens equally. Concretely, let the input prompt contain  $T$  tokens, of which  $T_v = |\mathcal{I}_v|$  correspond to vision tokens, where  $\mathcal{I}_v \subseteq \{1, \dots, T\}$  denotes the indices of vision tokens. We present the learning approach for adapting the value token representations  $V^{(h)}$ . Later in the section we justify this choice and consider alternatives. For a given attention head, we learn to update the vision token representations only

$$\tilde{v}_j^{(h)} = v_j^{(h)} + \Delta v_j^{(h)}; \quad \text{where } \Delta v_j^{(h)} := 0 \text{ for } j \notin \mathcal{I}_v$$

and each  $\Delta v_j^{(h)}$  is learned via LoRA as described next.

**Selected Heads Only.** Second, we apply updates to only a subset of attention heads rather than all heads. This provides finer control—adapting only those heads most relevant to the task while leaving others unchanged. Let  $\mathcal{H}^{\text{chosen}} \subseteq \{1, \dots, H\}$  be the set of selected heads (see Section 3.3 for specific head selection criteria) and  $N^{\text{chosen}} = |\mathcal{H}^{\text{chosen}}|$ .

Combining the two ideas above, we propose to learn parameters  $\Delta W_V^{(h)}$  such that

$$\tilde{V}^{(h)} = XW_V^{(h)} + \gamma_h M X \Delta W_V^{(h)},$$

where  $\gamma_h = \mathbb{I}[h \in \mathcal{H}^{\text{chosen}}]$  and  $M \in \{0, 1\}^{T \times T}$  is a diagonal matrix with  $M_{i,i} = \mathbb{I}[i \in \mathcal{I}_v]$ . This matrix formulation is provided for clarity; in practice, we parameterize  $\Delta W_V^{(h)}$  using a LoRA decomposition:

$$\Delta W_V^{(h)} = AB^{(h)}s, \quad s = \frac{\alpha}{r} \gamma \nu(N^{\text{chosen}}),$$

where  $A \in \mathbb{R}^{d_{\text{hidden}} \times r}$  and  $B^{(h)} \in \mathbb{R}^{r \times d_{\text{head}}}$  are learnable matrices, and the scaling factor  $s$  includes the normalization term  $\nu(N^{\text{chosen}})$ , which we describe next. In our implementation,  $A$  is shared across heads within a layer, while

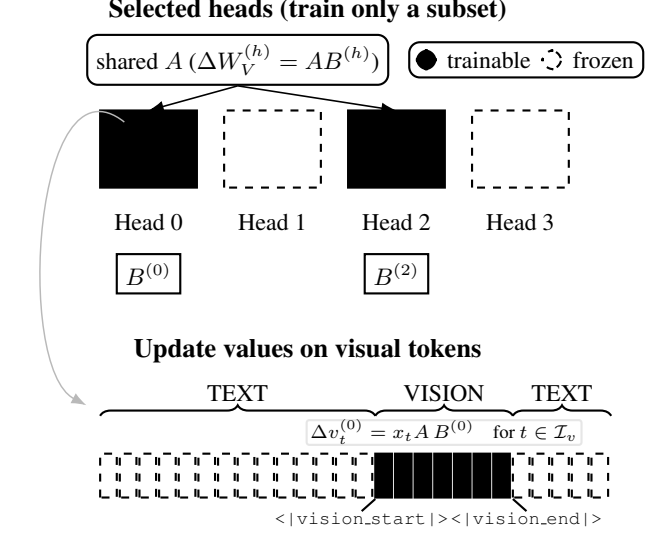


Figure 3. **Top:** Share one  $A$  per layer across its selected heads; learn  $B^{(h)}$  only for the selected heads. **Bottom:** For the selected heads, we update the *value* vectors  $v_t$  of the attention layer only on the visual-token span  $\mathcal{I}_v$  and not on the text-token positions.

$B^{(h)}$  is head-specific, motivated by two factors: (1) since  $d_{\text{hidden}} \gg d_{\text{head}}$ <sup>1</sup>, sharing  $A$  across a layer greatly reduces parameters and training FLOPs (detailed numbers for both 7B and 72B models in our ablation studies), and (2) head-specific parameters are required for the head-selection algorithm to compute per-head influence scores.

**Head-selection Normalization.** The standard LoRA activates *all* heads per layer, so the per-layer update magnitude is comparable across layers. With head selection, the number of chosen heads in a layer varies. To prevent the summed increment from growing with the number of chosen heads, we additionally apply a *selection size normalization*:

$$\nu(N^{\text{chosen}}) = \frac{1}{\sqrt{N^{\text{chosen}}}}.$$

This design follows from a variance-preserving argument that ensures the variance of  $\sum_{h \in \mathcal{H}^{\text{chosen}}} \Delta V^{(h)}$  remains invariant with respect to the number of chosen heads, assuming uncorrelated heads. See Section A.2 of the Appendix for more details.

**Projection Selectivity.** The standard LoRA can be applied to any of the query  $Q^{(h)}$ , key  $K^{(h)}$ , value  $V^{(h)}$  or output  $O^{(h)}$  representations. If we restrict the analysis to a single layer, updating the  $Q^{(h)}$  or  $O^{(h)}$  representations of vision tokens does not influence the output representations

<sup>1</sup>For example, in Qwen2.5-VL-7B,  $d_{\text{hidden}} = 3584$ ,  $d_{\text{head}} = 128$ .

of text tokens. This is because

$$o_i^{(h)} = \text{softmax} \left( \frac{q_i^{(h)} K^{(h)\top}}{\sqrt{d_k}} + \text{Mask}_i \right) V^{(h)},$$

and thus  $o_i^{(h)}$  depends only on the query for the token at  $i$ , together with the shared keys  $K^{(h)}$  and values  $V^{(h)}$ . Consequently, modifying  $q_j^{(h)}$  or  $o_j^{(h)}$  for any vision token at  $j \in \mathcal{I}_v$  has no effect on the output  $o_i^{(h)}$  of any text token at  $i \notin \mathcal{I}_v$ . On the other hand,  $V^{(h)}$  and  $K^{(h)}$  determine ‘what to look’ and ‘where to look’ in the image respectively, from the perspective of text tokens, and updating  $V^{(h)}$  and  $K^{(h)}$  solely on the vision tokens is more aligned with our goals. Based on our ablations, we find that updating the value representation  $V^{(h)}$  of vision tokens yields the optimal performance and outperforms alternatives such as updating only  $K^{(h)}$  or both  $K^{(h)}$  and  $V^{(h)}$ .

**Summary of Differences.** Compared to the standard LoRA, Image-LoRA (i) applies updates only to visual tokens, reducing adapter-only training FLOPs by skipping computation over both the input prompt text and output answer text, (ii) adapts only a subset of selected heads, with selection-size normalization to stabilize the magnitude of layer-wise updates, and (iii) shares  $A$  while keeping  $B^{(h)}$  head-specific, so the parameter count scales with  $|\mathcal{H}^{\text{chosen}}|$  instead of  $H$ , and the head-specific  $B$  enables head selection. These design choices yield substantial parameter and adapter-only training FLOP reductions while effectively modulating value representations. Relative to the standard LoRA, our approach reduces the FLOPs by a factor of  $O(T_v/T \times |\mathcal{H}^{\text{chosen}}|/H)$ .

### 3.3. Head Selection

**First-order Head Importance Estimation.** Our goal is to identify the attention heads  $h$  in the model that would most effectively reduce the training loss when their value matrices  $V^{(h)}$  are updated. A naïve way to rank heads is to modify one head at a time, recompute the loss for all samples, and select the heads that yield the largest decrease. However, this finite-difference procedure is prohibitively expensive. Instead, we adopt a first-order Taylor approximation that scores *all* heads in one backward pass. For parameters  $\theta$  and loss  $\ell$ , the first-order Taylor expansion gives

$$\Delta\ell = \ell(\theta + \delta\theta) - \ell(\theta) \approx \langle \nabla_\theta \ell, \delta\theta \rangle,$$

where higher-order terms  $O(\|\delta\theta\|^2)$  are neglected. Choosing the steepest direction of descent  $\delta\theta = -\nabla_\theta \ell$  leads to a change in loss as

$$\Delta\ell \approx -\|\nabla_\theta \ell\|_F^2$$

Thus,  $\|\nabla_\theta \ell\|_F^2$  can be used as a measure of the sensitivity of the loss to parameters  $\theta$ .

**Head Importance.** To measure the importance of each head, we adopt a setup analogous to the Image-LoRA factorization described in §3.2. Following standard practice, we initialize  $A$  with Gaussian noise and set  $B^{(h)}$  to zeros, with  $\gamma = 1$  and LoRA rank  $r = 1$  for efficiency. The importance of head  $h$  is then defined as

$$I(h) = \|\nabla_{B^{(h)}} \ell\|_F^2$$

which we refer to as the *influence score*. Since  $A$  is shared and frozen while  $B^{(h)}$  is head-specific and trainable, the gradient magnitude on  $B^{(h)}$  directly reflects how influential that head is.

**Head Diversity.** Besides importance, we consider a diversity factor, which we found beneficial in our experiments:

$$F(h) = (\nabla_{B^{(h)}} \ell) \odot (\nabla_{B^{(h)}} \ell),$$

where  $\odot$  denotes the Hadamard (element-wise) product.

**Head Selection Procedure.** We next select a subset of heads that balances importance and diversity. To determine the number of heads to select from each layer, we first compute the aggregate importance of layer  $L$  and convert it into a normalized weighting that guides head allocation:

$$\Phi_L = \sum_{h \in L} I(h), \quad p_L = \frac{(\Phi_L)^\tau}{\sum_{L'} (\Phi_{L'})^\tau}$$

where  $\tau \geq 0$  is a temperature parameter controlling how strongly importance is concentrated across layers. Given a total budget of  $K_{\text{sel}}$  heads, we allocate a per-layer budget using  $p_L$  and then perform a simple selection within each layer with considering diversity  $F(h)$ ; See Appendix A.1 and Algorithm 1 for the full procedure.

## 4. Experiments

Our experiments test whether *Image-LoRA* can match the capabilities of the *standard LoRA* while using fewer trainable parameters and lower adapter-only FLOPs evaluated on grounded vision-text reasoning tasks. Particularly, we examine QWEN2.5-VL-7B & 72B and LLaVA-NeXT-7B on ScreenSpot-Pro [14], RefCOCO [12], GSM8K [5], and ViLP [15] datasets. Then, we conduct extensive ablation studies on the design choices for Image-LoRA to demonstrate the effectiveness of our head-selection algorithm, the need of layer-wise normalization, the inferior performance of adapting both  $K$  and  $V$  compared to  $V$  alone, and other design variants.

### 4.1. Image-LoRA vs. Standard LoRA

We evaluate *Image-LoRA* and *standard LoRA* sweeping from text-heavy to image-heavy settings. We primarily study QWEN2.5-VL-7B and QWEN2.5-VL-72B on

ScreenSpot-Pro and RefCOCO, whose vision encoders allow accurate control of the image token numbers to yield different sceneries. To verify that Image-LoRA does not harm pure text reasoning, we also report empirical results on GSM8K, where the standard LoRA degrades performance while our Image-LoRA preserves the base model’s text reasoning capabilities. Moreover, evaluations on ViLP indicate that restricting adaptation to visual tokens might reduce shortcircuiting through language priors. Finally, we further test our approach on LLaVA-NEXT-7B.

**Controlling the input-text:image token ratio.** We control the ratio between number of input text tokens and number of image tokens by varying the image resolution while keeping the chat template fixed. As Qwen models tokenize images on a regular patch grid, the number of visual tokens,  $T_v$ , grows monotonically with the processed area. The text side effectively contains about  $T_{\text{text}} \approx 850$  tokens, mostly from system prompts, while each per-sample query remains short. The whole process only resamples the image while preserving its original aspect ratio as much as possible. See Section B.1 for more details.

**Task and Benchmarks.** For our main experiments, we consider a grounding task with a single-line target point\_2d: [x, y]; we optimize cross-entropy over this string. We report **Accuracy** as the fraction of predicted  $(x, y)$  that fall inside the ground-truth box in the model’s effective pixel space, and also report trainable parameters and adapter-only training FLOPs.

- **ScreenSpot-Pro [14] (UI grounding):** high-resolution interface screenshots paired with natural-language instructions and click/box annotations. Because screenshots are often  $> 3000 \times 2000$ , we use *image-heavy* input text:image ratios of 1:2, 1:3, 1:4, and 1:5. Average image token counts are in Table 1; example image resolutions per setting are in Table 6. We use a fixed random split: 1000 examples for *training + head selection* and the remaining 581 for *evaluation*.
- **RefCOCO [12] (referring expressions):** natural descriptions of target objects in COCO images with bounding boxes (and segmentations for a subset). As COCO images are relatively small ( $\approx 600 \times 640$ ), we use ratios of 1:1 and 1:1/2 (input text:image). We sample 2000 val examples for *training + head selection* and evaluate on 500 examples from test with no overlap.

**Training.** We compare our approach against the standard LoRA approach under different configurations.

- **Image-LoRA** adapts only the  $V$  projection in attention layers and only on visual-token spans, using rank  $r=8$  and scale  $\alpha=16$  without losing generality. For each

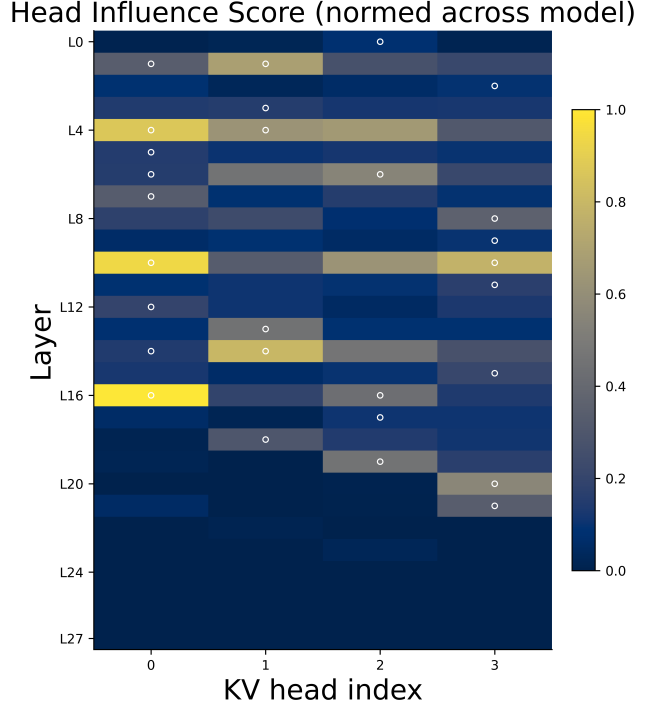


Figure 4. Head selection for Qwen2.5-VL-7B under a input-text:image token ratio of 1:2.

setting (i.e., different text:image ratio), we apply the proposed head selection strategy, choosing 28 out of 112 heads for QWEN2.5-VL-7B and 80 out of 640 for QWEN2.5-VL-72B. Note that 28 and 80 correspond to the number of layers in these models, respectively.

- The **standard LoRA (Std-LoRA)** baseline adapts  $Q$  and  $V$  on all attention heads and all tokens with the same  $r$  and  $\alpha$ . We choose  $Q, V$  because this is the most widely used configuration and is also the default setting in the official documentation. We also compare with the  $V$ -only Std-LoRA in terms of both FLOPs and performance, and further analyze other key configurations of standard LoRA in our ablation studies.

**Results.** Table 1 groups settings by dataset and ratio, and for each setting compares *Base (frozen)*, *Std-LoRA (QV, all tokens, all heads)*, and *Image-LoRA (V, visual tokens only, 28 heads)* in terms of accuracy, adapter FLOPs, and trainable parameters. Notably, the FLOPs of Image-LoRA are much lower than those of the standard LoRA, due to two factors: (1) using fewer heads via the proposed head selection algorithm, which reduces trainable parameters; and (2) computing only over the visual token span, excluding input prompts and output answers, which saves computation. This also yields the expected scaling behavior: Image-LoRA FLOPs are proportional to the image-token count (so  $1:4 \approx 2 \times 1:2$  and  $\approx 4 \times 1:1$ ), while Std-LoRA counts all tokens and thus scales with the overall sequence length

Table 1. **Main results across input text:image ratios.** FLOPs (G) denotes the total adapter-only training-time floating-point operations, measured in billions ( $10^{-9}$ ). The average fine-tuned parameter count for Image-LoRA for 7B and 72B models are, respectively, 629,781 and 3,011,629. The respective parameter counts for Std-LoRA are 2,523,192 and 16,384,160, respectively.

		QWEN2.5-VL-7B				QWEN2.5-VL-72B			
		SCREENSPOT-PRO		REFCOCO		SCREENSPOT-PRO		REFCOCO	
Text:Img Token Ratio	1:5	1:4	1:3	1:2	1:1	1:1/2	1:5	1:4	1:2
Avg #Image Tokens	4,195	3,367	2,534	1,677	851	426	4,195	3,367	1,677
Acc. (%)	Base	22.38	14.97	8.95	9.12	90.80	83.00	46.47	45.44
	Std-LoRA	37.18	30.12	<b>25.30</b>	<b>20.48</b>	93.40	<b>93.20</b>	58.18	54.04
	Image-LoRA	<b>37.35</b>	<b>30.98</b>	24.44	18.24	<b>93.60</b>	93.00	<b>58.35</b>	<b>55.94</b>
FLOPs (G)	Std-LoRA	76.53	63.99	51.38	38.38	25.86	19.42	496.9	415.5
	Image-LoRA	<b>15.85</b>	<b>12.72</b>	<b>10.03</b>	<b>6.63</b>	<b>3.36</b>	<b>1.61</b>	<b>75.80</b>	<b>59.49</b>
								<b>43.80</b>	<b>28.94</b>
								<b>15.05</b>	<b>7.54</b>

(prompt text + image + answer text). As a result, restricting adaptation to image tokens (i.e., our Image-LoRA) is particularly beneficial in settings with long textual contexts.

Since choosing  $QV$  for Std-LoRA adds FLOPs relative to  $V$ -only configuration, we also compare a  **$V$ -only Std-LoRA vs. our Image-LoRA**. On ScreenSpot-Pro, Image-LoRA reduces adapter-only FLOPs by 43.0%, 45.3%, 48.7%, and 54.6% at text:image ratios 1:5, 1:4, 1:3, and 1:2, respectively. Averaged over these settings, Image-LoRA yields a  $\approx 48\%$  FLOPs reduction (Detailed numbers are provided in Appendix B.2). These gains come from Image-LoRA’s design—fewer adapted heads with the proposed head selection algorithm and computation restricted to the visual-token span. Regarding performance,  $V$ -only Std-LoRA achieved consistent worse results than  $QV$  Std-LoRA, as shown in Table 4.

In terms of accuracy, Image-LoRA achieves comparable performance in image-heavy settings such as ScreenSpot-Pro (1:5, 1:4) and RefCOCO (1:1), while performing worse in those image-token less scenarios. The trainable parameters of Image-LoRA are approximately one-quarter those of Std-LoRA for 7B models and one-fifth for 72B models.

We show one example of our head selection for QWEN2.5-VL-7B in Figure 4, where the selected heads are distributed from the early layers to the middle-late layers. Similar patterns are observed in QWEN2.5-VL-72B. Due to space limitations, additional visualizations, analyses, and ablation studies are provided in Appendix B.1.

**Does Image-LoRA Affect Text Only Reasoning?** Because Image-LoRA applies adaptive weights only on the visual-token span, it does not interfere with language ability on pure-text inputs fundamentally. To show this empirically, we evaluate on the GSM8K [5] test set—a collection of 1,319 grade-school math word problems all in text form (no images). Qwen2.5-VL base attains 25.55%, and our Image-LoRA fine-tuned achieves the same 25.55%. In

contrast, a standard LoRA baseline fine-tuned on the same GSM8K data and text:image ratio drops to 24.79%. This result supports that Image-LoRA preserves pure-text reasoning while the standard LoRA, which updates all tokens, may degrade it.

**Can Image-LoRA Mitigate Overfitting to Language Priors?** Because Image-LoRA updates only the visual-token span, it might be less susceptible to overfitting language priors than Std-LoRA, which adapts parameters on all tokens. We evaluate this on ViLP [15], where each question is paired with three images: one whose answer can be inferred from the question text alone (“follow”) and two whose correct answers contradict the text prior and therefore require visual evidence (“against”). For example, for the question “Who is painting the Mona Lisa in the image?”, the text prior suggests *Leonardo da Vinci*, whereas the correct answer may be *Vincent van Gogh* depending on the image (Figure 2). Using the same backbone and hyper-parameters as in the main experiments, we fine-tune on the “follow” split and evaluate on the corresponding “against” images (i.e., same questions, out-of-distribution answers). Std-LoRA attains 5.00% accuracy, whereas Image-LoRA reaches 12.67%. The results suggest that constraining adaptation to visual tokens may help mitigate shortcutting via language priors.

**Applicability to Other VLMs.** We also evaluate LLaVA-NeXT-7B, comparing Image-LoRA with Std-LoRA. Because LLaVA-NeXT uses a quantized ViT grid with discrete high-resolution tiling, the image-token count changes only at tiling thresholds, which prevents precise control of the text:image token ratio; therefore we keep the original image resolution and match all other settings to the Qwen experiments. On ScreenSpot-Pro, accuracy remains near-zero before and after fine-tuning for both methods, so we report only RefCOCO. At the original resolution, the average to-

Table 2. **Head selection methods ablation on Qwen2.5-VL-7B.**All methods adapt  $K_{\text{sel}}=28$  heads. Entries are accuracy (%).

Method	1:5	1:4	1:3	1:2
Global-Rand	34.42	28.40	21.86	16.87
PerLayer-Rand	34.08	27.78	20.31	17.90
CorrMap	32.87	25.99	20.14	16.18
Ours	<b>37.35</b>	<b>30.98</b>	<b>24.44</b>	<b>18.24</b>

Table 3. **KV-budget ablation on Qwen2.5-VL-7B.** We vary  $K_{\text{sel}} \in \{1, 7, 28, 112\}$ . Entries are accuracy (%).

Method	1:5	1:4	1:3	1:2
Base (frozen)	22.38	14.97	8.95	9.12
1 head	28.23	16.52	12.05	10.50
7 heads	30.81	24.27	18.42	15.15
28 heads (ours)	<b>37.35</b>	<b>30.98</b>	24.44	18.24
112 heads	35.11	28.57	<b>25.82</b>	<b>19.28</b>

ken counts are  $T_{\text{text}}=133.4$  and  $T_v=2276.3$ . The LLaVA-v1.6-Mistral-7B base achieves 13% on the RefCOCO test set; Std-LoRA reaches 91.2% and Image-LoRA 92.0%. The corresponding trainable parameters are 3,407,936 (Std-LoRA) vs. 786,454 (Image-LoRA), and training FLOPs are 49.49 and 10.74 G, respectively. These results indicate that Image-LoRA remains competitive for LLaVA-NeXT architecture.

## 4.2. Ablations on Image-LoRA

We examine Image-LoRA designs in terms of (1) head-selection strategy, (2) how the head budget affects performance, (3) whether further adapting  $K$  on top of  $V$  brings additional benefits, (4) the types of layer-wise normalization, and (5) how parameters and FLOPs change when we not share A cross a layer. All experiments are conducted on the Qwen2.5-VL-7B model with rank  $r=8$ , LoRA scale  $\alpha=16$ , ScreenSpot-Pro dataset, and the same training hyperparameters as in the main experiments.

**Head Selection Strategy.** We compare our head selection strategy against the following baselines – *Global-Rand*: randomly sample 28 heads from the full model, *PerLayer-Rand*: sample exactly one head per layer (a total 28 heads), and a correlation-map heuristic (*CorrMap*) inspired by grounding saliency: we compute per-head correlation maps by comparing each attention head’s image-token attention to the ground-truth region across samples, derive a per-head alignment score from these maps, and select the 28 heads with the highest scores for later use (details in Appendix B.2). The results are shown in Table 2, demonstrating that our proposed approach consistently achieves the highest scores across all the ratios.

Table 4. **Updating  $K$  in ImageLoRA + different LoRA keys for Std-LoRA.** Entries are accuracy (%). Image-LoRA with  $V$  only is our proposed method.

Method	Adapters	1:5	1:4	1:3	1:2
Image-LoRA	$K$ only	29.60	24.10	19.10	13.77
Image-LoRA	$V+K$	34.77	25.65	22.20	15.49
Image-LoRA	$V$ only	<b>37.35</b>	<b>30.98</b>	24.44	18.24
Std-LoRA	$QKVO$	34.77	28.74	<b>25.30</b>	<b>21.51</b>
Std-LoRA	$V$	35.28	29.60	24.78	19.45
Std-LoRA	$QV$	37.19	30.12	<b>25.30</b>	20.48

Table 5. **Effect of selection-size normalization on Qwen2.5-VL-7B.** All runs use the proposed head selection procedure,  $K_{\text{sel}}=28$ ,  $V$ -only,  $r=8$ . Entries are accuracy (%).

Normalization	1:5	1:4	1:3	1:2
None ( $\nu(S)=1$ )	34.60	29.43	23.41	17.73
Linear ( $\nu(S)=1/S$ )	35.97	27.71	24.44	17.21
Ours ( $\nu(S)=1/\sqrt{S}$ )	<b>37.35</b>	<b>30.98</b>	<b>24.44</b>	<b>18.24</b>

**Number of Chosen Heads.** We vary the KV-head budget while keeping the selection method fixed to our one-shot influence head-selection algorithm. Qwen2.5-VL-7B has 28 layers and 112 KV heads in total, and we sweep among  $\{1, 7, 28, 112\}$  heads. As shown in Table 3, accuracy generally increases with more heads; however, more is not always better—at ratios 1:5 and 1:4, selecting 28 heads outperforms using all 112 heads, highlighting the effectiveness of our proposed selection algorithm.

**Updating  $K$  in addition to  $V$ .** Following the discussion in Section 3.2-Projection Selectivity, we test adding LoRA on the  $K$  path in addition to the  $V$  path on visual tokens, where we observe performance degradation compared to the  $V$ -only, as shown in the upper half of Table 4 for both  $K$  only and  $V+K$  configurations.

**Different keys for Std-LoRA.** For Std-LoRA, we further explore the  $V$ -only variant and  $QKVO$  variant on top of the  $QV$  configuration studied previously. As shown in the lower half of Table 4, Std-LoRA with  $QV$  achieves the best performance across most settings. We list more information, such as trainable parameters, in Appendix B.2.

**Selection-size Normalization.** With head selection, the number of adapted heads per layer  $N_{\text{chosen}}$  varies, so the raw LoRA increment  $\sum_{h \in \mathcal{H}_{\text{chosen}}} \Delta V^{(h)}$  can grow with  $N_{\text{chosen}}$ . We therefore scale the per-layer update as  $s = \frac{\alpha}{r} \gamma \nu(N_{\text{chosen}})$ , and compare two choices for  $\nu(\cdot)$ : **None** ( $\nu(S)=1$ ), which lets the expected update energy grow  $\propto N_{\text{chosen}}$ , and **Linear** ( $\nu(S)=1/S$ ), which keeps the

summed increment roughly constant but shrinks expected energy as  $\propto 1/N^{\text{chosen}}$ . None-normalization tends to over-scale layers where many heads are selected, while Linear-normalization may over-dampen layers with numerous selected heads. Both typically yield lower accuracy than our proposed  $\nu(S)=1/\sqrt{S}$ , as verified in Table 5.

**Effect of sharing  $A$ .** Sharing  $A$  across heads within each layer reduces adapter-only training FLOPs and parameters on ScreenSpot-Pro across a range of text:image token ratios. With Qwen2.5-VL-7B, the average adapter-only FLOPs drop by  $\approx 21.1\%$  and the parameter count by a similar fraction ( $\approx 172,032$  fewer). With Qwen2.5-VL-72B, the average FLOPs reduction is  $\approx 26.7\%$  with a comparable parameter decrease of  $\approx 26.6\%$  ( $\approx 1,064,960$  fewer).

## 5. Limitations and Discussions

The proposed Image-LoRA introduces fundamental challenges for batching, as image-token and text-token lengths vary across samples and must be handled efficiently. Both training and inference further demand substantial kernel-level and hardware-level optimizations to achieve competitive throughput. In particular, because Image-LoRA applies updates only to visual-token spans, designing an efficient inference pathway becomes crucial: in its current form, Image-LoRA must dynamically locate visual-token spans for every inference sample. This behavior differs fundamentally from Std-LoRA, which merges weights before inference without requiring such runtime checks.

Image-LoRA is most naturally applicable to transformer-based VLMs that represent images as explicit visual-token sequences. For architectures such as Llama-3.2-Vision [16], which integrate visual information via cross-attention directly into the text representation, Image-LoRA behaves much more like Std-LoRA, since the notion of a distinct visual-token span becomes less well-defined.

Regarding experimental scale, our current results are limited to on the order of a thousand samples due to constrained compute and the need to validate multiple components. A more comprehensive evaluation would ideally follow the large-scale setting of Schulman and Lab [18], which employs extensive data and dense sweeps over experimental settings, such as LoRA-rank variations.

Moreover, a detailed analysis of how Image-LoRA reshapes attention patterns across heads and layers—and how these patterns differ from those induced by Std-LoRA—could clarify its underlying mechanisms and inform further improvements. Beyond that, an open question is whether the dynamics of these pattern changes during training differ between Image-LoRA and Std-LoRA.

Finally, understanding the interaction between Image-LoRA and head selection is an important avenue for fu-

ture work. Our head-selection procedure is central to reducing the number of trainable parameters and, consequently, adapter-only FLOPs. It would be valuable to study how the selected heads evolve over the course of Image-LoRA training, particularly in web-scale settings where different subsets of attention heads may be optimal at different training stages. Moreover, this paper does not systematically examine how different head-selection methods affect performance: we focus on a single, simple head-selection scheme, and alternative criteria may lead to substantially different accuracy–efficiency trade-offs.

## 6. Conclusion

We presented *Image-LoRA*, a simple PEFT recipe for transformer-based VLMs that restricts adaptation to visual tokens and a small subset of attention heads selected by a one-shot influence score, with a layer normalization to stabilize updates. Across screen-centric grounding and referring setups spanning a range of text:image token ratios, Image-LoRA matched or approached standard LoRA while using fewer trainable parameters and lower adapter-only FLOPs. It preserved text-only reasoning while showing signs of reduced reliance on language priors. Despite being evaluated on limited backbones and tasks, we hope this vision-focused PEFT recipe inspires broader exploration.

## 7. Acknowledgment

The work was completed during Tiange’s internship at LG AI Research and was supported by computational resources from the University of Michigan.

## References

- [1] Ingeol Baek, Hwan Chang, Sunghyun Ryu, and Hwanhee Lee. How do large vision-language models see text in image? unveiling the distinctive role of ocr heads. *arXiv preprint arXiv:2505.15865*, 2025. 1
- [2] Qingqing Cao, Bhargavi Paranjape, and Hannaneh Hajishirzi. Pumer: Pruning and merging tokens for efficient vision language models. *arXiv preprint arXiv:2305.17530*, 2023. 3
- [3] Liang Chen, Haozhe Zhao, Tianyu Liu, Shuai Bai, Junyang Lin, Chang Zhou, and Baobao Chang. An image is worth 1/2 tokens after layer 2: Plug-and-play inference acceleration for large vision-language models. In *European Conference on Computer Vision*, pages 19–35. Springer, 2024. 3
- [4] Jiale Cheng, Yusen Liu, Xinyu Zhang, Yulin Fei, Wenyi Hong, Ruiliang Lyu, Weihan Wang, Zhe Su, Xiaotao Gu, et al. Glyph: Scaling context windows via visual-text compression. *arXiv e-prints*, pages arXiv–2510, 2025. 1
- [5] Karl Cobbe, Vineet Kosaraju, Mohammad Bavarian, Mark Chen, Heewoo Jun, Lukasz Kaiser, Matthias Plappert, Jerry Tworek, Jacob Hilton, Reiichiro Nakano, Christopher Hesse, and John Schulman. Training verifiers to solve math word problems. *arXiv preprint arXiv:2110.14168*, 2021. 1, 2, 5, 7

[6] Zihao Fu, Haoran Yang, Anthony Man-Cho So, Wai Lam, Lidong Bing, and Nigel Collier. On the effectiveness of parameter-efficient fine-tuning. In *Proceedings of the AAAI conference on artificial intelligence*, pages 12799–12807, 2023. 3

[7] Peng Gao, Jiaming Han, Renrui Zhang, Ziyi Lin, Shijie Geng, Aojun Zhou, Wei Zhang, Pan Lu, Conghui He, Xiangyu Yue, et al. Llama-adapter v2: Parameter-efficient visual instruction model. *arXiv preprint arXiv:2304.15010*, 2023. 3

[8] Demi Guo, Alexander M Rush, and Yoon Kim. Parameter-efficient transfer learning with diff pruning. *arXiv preprint arXiv:2012.07463*, 2020. 3

[9] Edward J Hu, yelong shen, Phillip Wallis, Zeyuan Allen-Zhu, Yuanzhi Li, Shean Wang, Lu Wang, and Weizhu Chen. LoRA: Low-rank adaptation of large language models. In *International Conference on Learning Representations*, 2022. 1, 3

[10] Aaron Jaech, Adam Kalai, Adam Lerer, Adam Richardson, Ahmed El-Kishky, Aiden Low, Alec Helyar, Aleksander Madry, Alex Beutel, Alex Carney, et al. Openai o1 system card. *arXiv preprint arXiv:2412.16720*, 2024. 2

[11] Seil Kang, Jinyeong Kim, Junhyeok Kim, and Seong Jae Hwang. Your large vision-language model only needs a few attention heads for visual grounding. In *Proceedings of the Computer Vision and Pattern Recognition Conference*, pages 9339–9350, 2025. 1, 3

[12] Sahar Kazemzadeh, Vicente Ordonez, Mark Matten, and Tamara Berg. ReferItGame: Referring to objects in photographs of natural scenes. In *Proceedings of the 2014 Conference on Empirical Methods in Natural Language Processing (EMNLP)*, pages 787–798, Doha, Qatar, 2014. Association for Computational Linguistics. 2, 5, 6

[13] Samir Khaki, Xiuyu Li, Junxian Guo, Ligeng Zhu, Chenfeng Xu, Konstantinos N Plataniotis, Amir Yazdanbakhsh, Kurt Keutzer, Song Han, and Zhijian Liu. Sparselora: Accelerating llm fine-tuning with contextual sparsity. *arXiv preprint arXiv:2506.16500*, 2025. 3

[14] Kaixin Li, Ziyang Meng, Hongzhan Lin, Ziyang Luo, Yuchen Tian, Jing Ma, Zhiyong Huang, and Tat-Seng Chua. Screenspot-pro: Gui grounding for professional high-resolution computer use. *arXiv preprint arXiv:2504.07981*, 2025. 2, 5, 6

[15] Tiange Luo, Ang Cao, Gunhee Lee, Justin Johnson, and Honglak Lee. Probing visual language priors in VLMs. In *Forty-second International Conference on Machine Learning*, 2025. 1, 2, 5, 7

[16] AI Meta. Llama 3.2: Revolutionizing edge ai and vision with open, customizable models. *Meta AI Blog*. Retrieved December, 20:2024, 2024. 9

[17] Paul Michel, Omer Levy, and Graham Neubig. Are sixteen heads really better than one? *Advances in neural information processing systems*, 32, 2019. 3

[18] John Schulman and Thinking Machines Lab. Lora without regret. *Thinking Machines Lab: Connectionism*, 2025. <https://thinkingmachines.ai/blog/lora/>. 1, 3, 9

[19] Reece Shuttleworth, Jacob Andreas, Antonio Torralba, and Pratyusha Sharma. Lora vs full fine-tuning: An illusion of equivalence. *arXiv preprint arXiv:2410.21228*, 2024. 3

[20] Yi-Lin Sung, Varun Nair, and Colin A Raffel. Training neural networks with fixed sparse masks. *Advances in Neural Information Processing Systems*, 34:24193–24205, 2021. 3

[21] Yi-Lin Sung, Jaemin Cho, and Mohit Bansal. VI-adapter: Parameter-efficient transfer learning for vision-and-language tasks. In *Proceedings of the IEEE/CVF conference on computer vision and pattern recognition*, pages 5227–5237, 2022. 3

[22] Elena Voita, David Talbot, Fedor Moiseev, Rico Sennrich, and Ivan Titov. Analyzing multi-head self-attention: Specialized heads do the heavy lifting, the rest can be pruned. *arXiv preprint arXiv:1905.09418*, 2019. 3

[23] Han Wang, Yongjie Ye, Bingru Li, Yuxiang Nie, Jinghui Lu, Jingqun Tang, Yanjie Wang, and Can Huang. Vision as lora. *arXiv preprint arXiv:2503.20680*, 2025. 3

[24] Haoran Wei, Yaofeng Sun, and Yukun Li. Deepseek-ocr: Contexts optical compression. *arXiv preprint arXiv:2510.18234*, 2025. 1

[25] Senqiao Yang, Yukang Chen, Zhuotao Tian, Chengyao Wang, Jingyao Li, Bei Yu, and Jiaya Jia. Visionzip: Longer is better but not necessary in vision language models. In *Proceedings of the Computer Vision and Pattern Recognition Conference*, pages 19792–19802, 2025. 3

[26] Elad Ben Zaken, Shauli Ravfogel, and Yoav Goldberg. Bitfit: Simple parameter-efficient fine-tuning for transformer-based masked language-models. *arXiv preprint arXiv:2106.10199*, 2021. 3

[27] Maxime Zanella and Ismail Ben Ayed. Low-rank few-shot adaptation of vision-language models. In *Proceedings of the IEEE/CVF Conference on Computer Vision and Pattern Recognition*, pages 1593–1603, 2024. 3

[28] Jiarui Zhang, Mahyar Khayatkhoei, Prateek Chhikara, and Filip Ilievski. Mllms know where to look: Training-free perception of small visual details with multimodal llms. *arXiv preprint arXiv:2502.17422*, 2025. 3

[29] Qingru Zhang, Minshuo Chen, Alexander Bukharin, Nikos Karmpatiakis, Pengcheng He, Yu Cheng, Weizhu Chen, and Tuo Zhao. Adalora: Adaptive budget allocation for parameter-efficient fine-tuning. *arXiv preprint arXiv:2303.10512*, 2023. 3

[30] Yuan Zhang, Chun-Kai Fan, Junpeng Ma, Wenzhao Zheng, Tao Huang, Kuan Cheng, Denis Gudovskiy, Tomoyuki Okuno, Yohei Nakata, Kurt Keutzer, et al. Sparsevlm: Visual token sparsification for efficient vision-language model inference. *arXiv preprint arXiv:2410.04417*, 2024. 3

[31] Mengjie Zhao, Tao Lin, Fei Mi, Martin Jaggi, and Hinrich Schütze. Masking as an efficient alternative to fine-tuning for pretrained language models. *arXiv preprint arXiv:2004.12406*, 2020. 3

[32] Zhuofan Zong, Bingqi Ma, Dazhong Shen, Guanglu Song, Hao Shao, Dongzhi Jiang, Hongsheng Li, and Yu Liu. Mova: Adapting mixture of vision experts to multimodal context. *Advances in Neural Information Processing Systems*, 37:103305–103333, 2024. 3

## A. Method Details

### A.1. Head Selection Procedure (details)

**Visual-only gradients & Different ratios** For our head selection procedure, gradients are restricted to the visual token slice when estimating the head importance score  $I(h)$  and head diversity feature  $F(h)$  for each head  $h$ . For the same model but different input text:image token ratios, we run the head selection procedure once for each ratio.

**Layerwise budgeting.** Using the per-head importance  $I(h)$  defined in the main text, we first accumulate per-layer mass  $\Phi_L = \sum_{h \in L} I(h)$  and form normalized allocation weights  $p_L = \frac{\Phi_L^\tau}{\sum_{L'} \Phi_{L'}^\tau}$  with temperature  $\tau \geq 0$ , so that  $p_L$  encodes the fraction of the global head budget assigned to layer  $L$  (and  $\sum_L p_L = 1$ ). Briefly,  $\tau = 0$  yields uniform-by-layer allocation;  $\tau = 1$  is proportional to mass (linear); and  $\tau \in (0, 1)$  compresses differences in layer mass (still favoring high-mass layers, but more gently). In our experiments as shown in Appendix B.1, we find  $\tau = 0.5$  to be a balanced choice. Given a global budget of  $K_{\text{sel}}$  heads (like  $K_{\text{sel}} = 28$  we used in the main experiment), these allocation weights  $p_L$  define target per-layer quotas. We first compute initial rounded quotas  $\tilde{k}_L = \lfloor K_{\text{sel}} p_L + \frac{1}{2} \rfloor$ , cap each by capacity  $H$ ,

$$k_L \leftarrow \min(\tilde{k}_L, H),$$

then greedily adjust  $\{k_L\}$  so that  $\sum_L k_L = K_{\text{sel}}$  exactly: if  $\sum_L k_L < K_{\text{sel}}$  we add heads to layers in descending order of  $\Phi_L$  while respecting capacities; if  $\sum_L k_L > K_{\text{sel}}$  we remove heads from layers in ascending order of  $\Phi_L$  until the sum matches. (When  $\sum_L \Phi_L = 0$ , we fall back to capacity-proportional  $p_L$ .) The resulting  $\{k_L\}$  are the per-layer budgets used by the within-layer candidate selection step described next.

**Candidate pool and diversity-aware selection.** Within layer  $L$ , given its budget  $k_L$ , we first assemble a candidate pool

$$k'_L = \min(H, \lceil \rho k_L \rceil), \quad P_L = \text{Top}_{k'_L} \{I(h) : h \in L\},$$

where  $\rho \geq 1$  is an expansion factor and  $I(h)$  is the importance score from the main text. As  $\rho \rightarrow 1^+$ , selection becomes primarily importance-driven; at  $\rho = 1$  it reduces to pure top- $k$  by importance within layer  $L$ . We set  $\rho = 2$  for our main experiments and studied it in our ablation experiments. To discourage near-duplicates, we use the head diversity feature  $F(h) = (\nabla_{B^{(h)}} \ell) \odot (\nabla_{B^{(h)}} \ell)$  (also defined in Section 3.3) and perform *cosine farthest-first* selection on row-normalized  $\{F(h) : h \in P_L\}$ : initialize with the highest-importance head from  $P_L$ , then iteratively add the candidate that maximizes its minimum cosine distance

to the already-selected set. This returns a diverse subset  $\mathcal{H}_{\text{chosen}}^{(L)}$  of size  $k_L$ . We show the importance of including the diversity term in the experimental results presented in the Appendix B.1.

---

**Algorithm 1** Head selection via Head Influence Scores Estimation

---

**Require:** probe set  $\mathcal{D}$ , global KV budget  $K_{\text{sel}}$ , temperature  $\tau$ , diversity multiplier  $\rho$

- 1: **for** each layer  $L$  **do**
- 2:     rank-1 approximation: shared  $A^{(L)} \in \mathbb{R}^{d_{\text{hidden}} \times 1}$ , per-KV  $B_j^{(L)} \in \mathbb{R}^{1 \times d_{\text{head}}}$ ; freeze base, set  $\gamma^{(L)} \leftarrow 1$ ; restrict gradients to the visual token slice.
- 3:     initialize importance  $I_j^{(L)} \leftarrow 0$  and diversity feature  $F_j^{(L)} \leftarrow 0$  for  $j=1, \dots, H_{kv}^{(L)}$ .
- 4: **for** each  $(X, y) \in \mathcal{D}$  **do**
- 5:     forward with CE loss; one backward pass
- 6:     **for** each layer  $L$ , head  $j$  **do**
- 7:          $\Delta \leftarrow \nabla_{B_j^{(L)}} \ell \in \mathbb{R}^{d_{\text{head}}}$
- 8:          $I_j^{(L)} += \|\Delta\|_2^2; \quad F_j^{(L)} += \Delta^{\odot 2}$
- 9:     compute  $\Phi_L = \sum_j I_j^{(L)}$  and  $p_L = \Phi_L^\tau / \sum_{L'} \Phi_{L'}^\tau$   $\triangleright$  if  $\sum_{L'} \Phi_{L'} = 0$ , set  $p_L \propto H_{kv}^{(L)}$
- 10:     $\tilde{k}_L \leftarrow \lfloor K_{\text{sel}} p_L + \frac{1}{2} \rfloor; \quad k_L \leftarrow \min(\tilde{k}_L, H)$
- 11:    greedily adjust  $\{k_L\}$  so that  $\sum_L k_L = K_{\text{sel}}$  (add by descending  $\Phi_L$ ; remove by ascending  $\Phi_L$ )
- 12: **for** each layer  $L$  **do**
- 13:     form pool  $P_L$ : top  $\min(H, \lceil \rho k_L \rceil)$  by importance  $I_j^{(L)}$ ; row-normalize diversity features  $F_j^{(L)} \leftarrow F_j^{(L)} / \|F_j^{(L)}\|_2$
- 14:     select  $k_L$  heads from  $P_L$  via cosine farthest-first (initialized with the highest-importance head) on  $\{F_j^{(L)}\}$ , yielding  $\mathcal{H}_{\text{chosen}}^{(L)}$
- 15:     map KV  $\rightarrow$  Q (if grouped-query is used):  $\mathcal{H}_q^{(L)} \leftarrow \bigcup_{j \in \mathcal{H}_{\text{chosen}}^{(L)}} \Gamma^{(L)}(j)$
- 16: **return**  $\{\mathcal{H}_q^{(L)}\}_L$   $\triangleright$  selected Q-head sets used by Image-LoRA training

---

**Complexity.** The procedure requires one forward+backward pass per probe example with gradients confined to the visual slice. Storage per layer is  $O(H d_{\text{head}})$  for diversity features and  $O(H)$  for scalar scores. Farthest-first selection over the pool is  $O(k'_L d_{\text{head}})$  for a single sweep.

### A.2. Head-selection Normalization.

Standard LoRA implicitly activates *all* KV heads per layer, i.e.,  $N_{\text{chosen}} = H$ , so the per-layer update magnitude is implicitly comparable across layers. With head selection,

$N_{\text{chosen}}$  varies; to prevent the summed increment from growing with  $N_{\text{chosen}}$ , we scale the update as

$$s = \frac{\alpha}{r} \gamma \nu(N_{\text{chosen}}).$$

A variance-preserving choice follows from a simple energy argument. Let  $\Delta V^{(h)}$  be the per-head increment (for head  $j$ ) and suppose  $\mathbb{E}[\Delta V^{(h)}] = 0$  with  $\mathbb{E}[\|\Delta V^{(h)}\|_F^2] = \sigma_L^2$ , and approximate different heads as uncorrelated. Then

$$\mathbb{E} \left[ \left\| \sum_{h \in \mathcal{H}_{\text{chosen}}^{(L)}} \Delta V^{(h)} \right\|_F^2 \right] = N_{\text{chosen}} \sigma^2.$$

After scaling by  $\nu(N_{\text{chosen}})$ , the expected energy becomes  $\nu(N_{\text{chosen}})^2 N_{\text{chosen}} \sigma^2$ . Setting this equal to  $\sigma^2$  yields the variance-preserving rule

$$\nu(N_{\text{chosen}}) = \frac{1}{\sqrt{N_{\text{chosen}}}}.$$

If heads exhibit positive average pairwise correlation  $\rho$  (so  $\mathbb{E}[\langle \Delta V^{(i)}, \Delta V^{(j)} \rangle] \approx \rho \sigma^2$  for  $i \neq j$ ), the same calculation gives

$$\mathbb{E} \left[ \left\| \sum_{h \in \mathcal{H}_{\text{chosen}}^{(L)}} \Delta V^{(h)} \right\|_F^2 \right] \approx (N_{\text{chosen}} + \rho N_{\text{chosen}}(N_{\text{chosen}} - 1)) \sigma^2$$

and an energy-matching scale

$$\nu(N_{\text{chosen}}) = (N_{\text{chosen}} + \rho N_{\text{chosen}}(N_{\text{chosen}} - 1))^{-1/2}$$

When  $\rho$  is unknown, the  $\frac{1}{\sqrt{N_{\text{chosen}}}}$  rule is a robust approximation; the learned gate  $\gamma$  absorbs residual mismatch.

### A.3. Visual-token-only finetuning with unchanged attention.

Let the self-attention in layer  $L$  project inputs  $X \in \mathbb{R}^{T \times d_{\text{hidden}}}$  to  $V \in \mathbb{R}^{T \times H \times d_{\text{head}}}$  via  $v_{\text{proj}} : \mathbb{R}^{d_{\text{hidden}}} \rightarrow \mathbb{R}^{H d_{\text{head}}}$ . We adapt only the *value* ( $V$ ) path on the visual-token index set  $\mathcal{I}_v$ . The attention probabilities  $a_{i,j}^{(h)} = \text{softmax}_j(\langle q_i^{(h)}, k_j^{(h)} \rangle / \sqrt{d_{\text{head}}})$  remain unchanged, while the output becomes

$$\tilde{o}_i^{(h)} = \sum_j a_{i,j}^{(h)} \tilde{v}_j^{(h)}, \quad \tilde{v}_j^{(h)} = v_j^{(h)} + \Delta v_j^{(h)}.$$

Head-wise scaling of values by  $c_j$  satisfies

$$\sum_j a_{i,j}^{(h)} (c_j v_j^{(h)}) = \sum_j (c_j a_{i,j}^{(h)}) v_j^{(h)},$$

so modifying values is equivalent to multiplying attention weights without re-normalizing the softmax. In our ablation studies, we applied the modification to  $K$  before normalization—thus changing the probability distribution—and found that this consistently degraded performance. Restricting updates to  $\mathcal{I}_v$  also reduces training FLOPs roughly by  $T_v/T$ , which is substantial for text-heavy prompts.

### A.4. Grouped Query Attention (GQA)

For a transformer layer  $L$  with hidden width  $d_{\text{hidden}}$ , head dimension  $d_{\text{head}}$ ,  $H_q$  query heads and  $H_{kv}$  key/value heads, we assume grouped-query attention with grouping factor  $g$ , so that  $H_q = g H_{kv}$ . We denote the *selected* query heads by  $\mathcal{H}_q \subset \{0, \dots, H_q - 1\}$ , and their induced chosen KV heads by

$$\mathcal{H}_{\text{chosen}} = \{ \lfloor h/g \rfloor : h \in \mathcal{H}_q \}, \quad N_{\text{chosen}} \triangleq |\mathcal{H}_{\text{chosen}}|.$$

Thus, multiple query heads may share the same KV head;  $N_{\text{chosen}}$  counts the number of *unique* KV heads. We denote the visual-token index set by  $\mathcal{I}_v$  and its length by  $T_v = |\mathcal{I}_v|$ . Throughout, we use the KV index purely to address heads; we adapt  $V$  only in main experiments, while  $K$  is included only for ablation studies.

### A.5. Parameter Counts on QWEN2.5-VL-7B (GQA).

QWEN2.5-VL-7B uses grouped-query attention:  $H_q = 28$  query heads share  $H_{kv} = 4$  key/value heads (we use the KV index to address heads; only  $V$  is adapted). With  $d_{\text{hidden}}=3584$ ,  $d_{\text{head}}=128$ ,  $N_L=28$  layers, rank  $r=8$ , and an illustrative selection  $N_{\text{chosen}} = 4$  KV heads per layer:

$$\#A = d_{\text{hidden}} \times r = 3584 \times 8 = 28,672,$$

$$\#B^{(h)} = N_{\text{chosen}} \times r \times d_{\text{head}} = 4 \times 8 \times 128 = 4,096.$$

Including one scalar  $\gamma$  gives  $28,672 + 4,096 + 1 = 32,769$  parameters per layer and  $32,769 \times N_L = 917,532$  across the stack. The dominant  $d_{\text{hidden}} \times r$  term motivates sharing  $A$ ; head-specific  $B$  ( $r \times d_{\text{head}}$ ) preserves per-head expressivity at a cost proportional to  $N_{\text{chosen}}$ .

## B. Experimental Details

### B.1. Main Experiment

**Training details.** Image-LoRA adapters are injected *pre-RoPE* and *before cache updates*. Unless noted, rank  $r=8$ ,  $\alpha=16$ , no dropout, and LoRA parameters are in fp32. *Standard LoRA* follows the *QV* practice recommended in Qwen’s training docs<sup>2</sup>, i.e., it adapts the  $q$ - and  $v$ -projections on *all* tokens and *all* heads (no head selection, no visual-token only restriction), using the same rank  $r$  and scale  $\alpha$ . We train for 5 epochs with AdamW, learning rate  $5 \times 10^{-4}$ , batch size 8, and cosine lr scheduler. For Image-LoRA we share one  $A^{(L)} \in \mathbb{R}^{H \times r}$  per layer and fit head-specific  $B_{v,j}^{(L)} \in \mathbb{R}^{r \times d_{\text{head}}}$  only for selected KV heads; at inference we freeze  $\{A, B, \gamma\}$  and apply the same visual-slice update so non-visual tokens incur no additional compute. Head selection uses a fixed global budget of  $K_{\text{sel}} = 28$  KV heads across the 7B model. Since

<sup>2</sup>[https://qwen.readthedocs.io/en/latest/training/llama\\_factory.html](https://qwen.readthedocs.io/en/latest/training/llama_factory.html)

Table 6. **Example image resolutions for each input text:image token ratio.** The average image token counts (#Image Tokens) correspond to Table 1. We provide two example image resolutions for reference.

Ratio	#Image Tokens	Example Res. #1 (W×H)	Example Res. #2 (W×H)
ScreenSpot-Pro			
1:5	4,195	3472×952	2240×1456
1:4	3,367	3108×840	2072×1260
1:3	2,534	2660×756	1764×1092
1:2	1,677	2184×616	1540×840
RefCOCO			
1:1	851	1036×644	952×700
2:1	426	700×476	588×560

QWEN2.5-VL-7B has 28 layers and grouped-query attention with  $g=7$  ( $H_q=28 \Rightarrow H_{kv}=4$  per layer), selecting 28 KV heads amounts to a  $\frac{28}{28 \times 4} = 1/4$  fraction of all KV heads. For 72B model, we have  $K_{sel} = 80$ , where QWEN2.5-VL-72B has 80 layers and grouped-query attention with  $g=8$  ( $H_q=64 \Rightarrow H_{kv}=8$  per layer), selecting 80 KV heads amounts to a  $\frac{80}{80 \times 8} = 1/8$  fraction of all KV heads. The data used for head selection are always the same as the training set in each dataset (no risk of evaluation set leakage).

**Controlling the input-text:image token ratio details.** We control the ratio by sweeping the processed image resolution while keeping the chat template fixed. The visual span  $\mathcal{I}_v$  is delimited by  $<|\text{vision\_start}|> \dots <|\text{vision\_end}|>$ . As Qwen models tokenize images on a regular patch grid, the number of visual tokens,  $T_v$ , grows monotonically with the processed area. For QWEN2.5-VL with `patch_size=14` and `merge_size=2`, the effective stride is  $s = 28$  px and  $T_v \approx \left\lfloor \frac{H}{s} \right\rfloor \left\lfloor \frac{W}{s} \right\rfloor$ . The text side effectively contains about ( $T_{\text{text}} \approx 850$  tokens, mostly from system prompts, while each per-sample query remains short. Given a target ratio  $\rho := T_{\text{text}}/T_v$ , we set  $T_v^* \approx T_{\text{text}}/\rho$  and binary-search the processed longest side—bounded by `min_pixels/max_pixels` and quantized to multiples of  $s$ —until  $|T_v - T_v^*| \leq \varepsilon$ . The whole process only resamples the image while preserving its original aspect ratio as much as possible. It cannot achieve a perfectly fixed text:image token ratio for every sample since the resolution must be a multiple of 28, but it yields ratios that are very close across samples, enabling consistent sweeps from text-heavy to image-heavy supervision.

Table 7. **Ablations on layerwise budgeting  $\tau$  and diversity factor  $\rho$  on Qwen2.5-VL-7B.** Columns report accuracy (%) at different text:image token ratios. Defaults underlined ( $\tau = 0.5, \rho = 2.0$ ).

Method	1:5	1:4	1:3	1:2
<i>Layerwise budgeting (diversity-aware, <math>\rho = 2.0</math> fixed)</i>				
$\tau = 0$ (uniform-by-layer)	34.77	27.88	23.06	16.87
$\tau = \underline{0.5}$	<b>37.35</b>	<b>30.98</b>	<b>24.44</b>	18.24
$\tau = 1$ (mass-proportional)	35.11	28.40	23.92	<b>18.59</b>
<i>Diversity vs. importance-only (<math>\tau = 0.5</math> fixed)</i>				
Importance-only ( $\rho = 1$ )	35.11	28.40	23.75	17.9
Diversity-aware ( $\rho = 2.0$ )	<b>37.35</b>	<b>30.98</b>	<b>24.44</b>	<b>18.24</b>
Diversity-aware ( $\rho = 3.0$ )	34.08	29.09	22.55	16.52

**Head Selection Procedure More Analysis** We study two orthogonal knobs in our head-selection method: (i) the *layerwise budget temperature*  $\tau$ , which distributes the total head budget across layers (see Section 3.3 and Appendix A.1), and (ii) the *within-layer* selection rule (diversity-aware vs. importance-only), controlled by the pool expansion factor  $\rho$  (Appendix A.1). Unless stated otherwise, we select  $K_{sel} = 28$  KV heads out of  $H_{\text{tot}} = 112$  in Qwen2.5-VL-7B (28 layers  $\times$  4 KV heads per layer).

**Layerwise budgeting via  $\tau$ .** Recall that we aggregate per-layer importance  $\Phi_L = \sum_{h \in L} I(h)$  and form allocation weights  $p_L \propto \Phi_L^\tau$ , which are then converted into integer quotas  $k_L$  under a global budget  $K_{sel}$  (see Appendix A.1 for the exact rounding and correction scheme). Intuitively,  $\tau = 0$  yields an *approximately uniform* allocation across layers,  $\tau = 1$  makes the budget *proportional to mass*  $\Phi_L$ , and  $0 < \tau < 1$  *compresses* differences in  $\Phi_L$  while still favoring high-mass layers. We use  $\tau = 0.5$  as our default and additionally compare  $\tau \in \{0, 1\}$ . We list some head selection examples in Figure 10. For Qwen2.5-VL-7B with  $L = 28$  layers and  $K_{sel} = 28$ , the  $\tau = 0$  setting degenerates to  $k_L = 1$  for every layer (up to rounding), i.e., selecting exactly one KV head per layer—the one with the highest importance score.

**Diversity vs. importance-only.** Given a layerwise budget  $\{k_L\}$ , we ablate the within-layer selection rule. The *importance-only* baseline simply picks, in each layer  $L$ , the top- $k_L$  heads by importance score  $I(h)$ . The *diversity-aware* variant first forms a pool of size  $k'_L = \min(H_{kv}^{(L)}, \lceil \rho k_L \rceil)$  by taking the top- $k'_L$  heads in  $L$  by  $I(h)$ , and then applies cosine farthest-first selection on the diversity features  $F(h)$  (Section 3.3 and Appendix A.1) to obtain a diverse subset of size  $k_L$ . The expansion factor  $\rho \geq 1$  controls the trade-off:  $\rho = 1$  reduces exactly to pure top- $k_L$  by importance, while larger  $\rho$  allows more diversity at a small cost in  $I(h)$ . In our main experiments we fix  $\tau = 0.5$ .

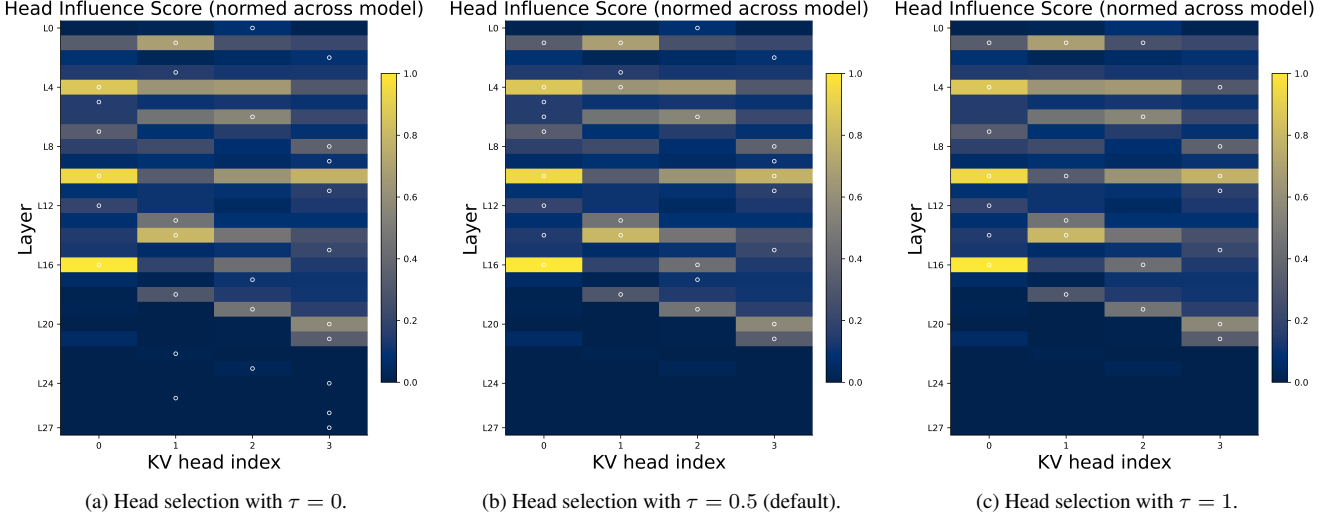


Figure 5. **Head selection patterns with different  $\tau$ .** The head selection procedure uses default hyper-parameters  $\rho = 2$ . All results are obtained on ScreenSpot-Pro using the 1:2 input-text:image token ratio. Intuitively,  $\tau = 0$  yields an *approximately uniform* allocation across layers, and  $\tau = 1$  makes the budget *proportional to mass*  $\Phi_L$ . We use  $\tau = 0.5$  in our main experiments. For Qwen2.5-VL-7B with 28 layers and  $K_{\text{sel}} = 28$ , the  $\tau = 0$  setting reduces to select exactly one KV head per layer — the one with the highest importance score.

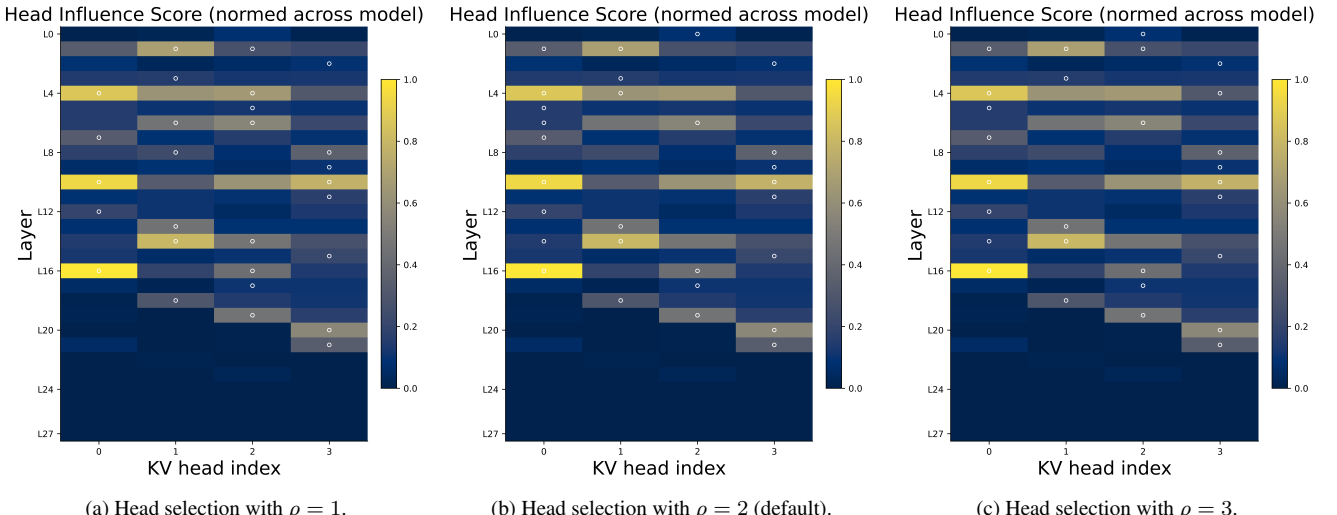


Figure 6. **Head selection patterns with different  $\rho$ .** The head selection procedure uses default hyper-parameters  $\tau = 0.5$ . All results are obtained on ScreenSpot-Pro using the 1:2 input-text:image token ratio. We use  $\rho = 2$  in our main experiments.  $\rho = 1$  reduces exactly to pure top- $k_L$  by importance, while larger  $\rho$  allows more diversity at a small cost in  $I(h)$ .

and compare (i) the importance-only baseline ( $\rho = 1$ ) and (ii) diversity-aware selection with  $\rho \in \{2.0, 3.0\}$ , where  $\rho = 2.0$  is our default setting. We list some head selection examples in Figure 6.

The results in Table 7 validate our choices for the main experiments, namely setting  $\tau = 0.5$  and  $\rho = 2.0$ .

## B.2. Ablation Studies

**More LoRA Ranks** We report the results for different LoRA ranks  $r = \{2, 8, 32\}$  in Table 8.

Table 8. **LoRA rank ablation on Qwen2.5-VL-7B.** All methods adapt  $K_{\text{sel}}=28$  heads. Entries are accuracy (%).

LoRA rank	1:5	1:4	1:3	1:2
$r = 2$	33.91	26.16	23.58	16.52
$r = 8$	37.35	30.98	24.44	18.24
$r = 32$	38.55	30.29	25.65	18.93

**More Parameters & FLOPs information** In the results analysis of Table 1, we report the FLOPs savings for

the Qwen-2.5-VL-7B model when comparing V-only Std-LoRA with our Image-LoRA. Here, we provide detailed information on the different Std-LoRA key configurations for both the 7B and 72B models, including trainable parameter counts and adapter-only training FLOPs. All methods adopt a LoRA rank of 8. The results are shown in Tables 9 and 10. Our Image-LoRA is applied solely to the value path  $V$  and to visual tokens, resulting in significantly lower adapter-only training FLOPs.

**Correlation-based Head Selection** For each image-instruction pair, we isolate the vision-token span and the set of query tokens, extract the attention tensor for every layer  $l$  and head  $h$ , average it over query positions to obtain a per-head image-attention map  $a_{l,h}^{(i)} \in \mathbb{R}^V$  (with  $V = g_h g_w$  vision tokens, each corresponding to a spatial cell in the vision tokenizer/encoder’s grid so that  $a_{l,h}^{(i)}$  can be interpreted as a coarse attention pattern over the image), and compute a Pearson-style correlation with the flattened ground-truth mask  $m^{(i)} \in \{0, 1\}^V$  by cosine on zero-mean vectors:

$$r_{l,h}^{(i)} = \left\langle \frac{a_{l,h}^{(i)} - \overline{a_{l,h}^{(i)}}}{\|a_{l,h}^{(i)} - \overline{a_{l,h}^{(i)}}\|_2}, \frac{m^{(i)} - \overline{m^{(i)}}}{\|m^{(i)} - \overline{m^{(i)}}\|_2} \right\rangle.$$

Across  $N$  samples this yields two heatmaps: the mean correlation  $r_{l,h} = \frac{1}{N} \sum_i r_{l,h}^{(i)}$  and the frequency  $p_{l,h} = \frac{1}{N} \sum_i \mathbf{1}[r_{l,h}^{(i)} > \tau]$  that the per-sample correlation exceeds a threshold  $\tau$  (default 0.3). We rank heads using a layer-normalized score that rewards both strength and consistency, e.g.

$$s_{l,h} = \text{ReLU}(z_l(r_{l,h})) \cdot p_{l,h},$$

where  $z_l(\cdot)$  z-scores within layer  $l$  to remove layer-scale effects. For models with grouped-query attention (GQA), let  $\mathcal{G}(l, k)$  denote the set of query heads tied to KV head  $k$  in layer  $l$ ; we collapse to KV granularity via

$$s_{l,k}^{\text{KV}} = \max_{h \in \mathcal{G}(l,k)} s_{l,h},$$

and select the 28 KV heads with the largest  $s_{l,k}^{\text{KV}}$  for subsequent use.

One visualization of the correlation-map-based selection is shown in Figure 8a. Compared to our proposed head-selection procedure (Figure 8b, under ratio 1:2), it tends to concentrate more heavily on a few middle-late layers.

**More Head Selection Results & Studies** We list more visualizations for our head selection results, including one 72B model selection (Figure 7), one LLaVA-Next-7B selection (Figure 9), the head selections with different head budgets (Figure 5), and the head selections under different input-text:image token ratios (Figure 11).

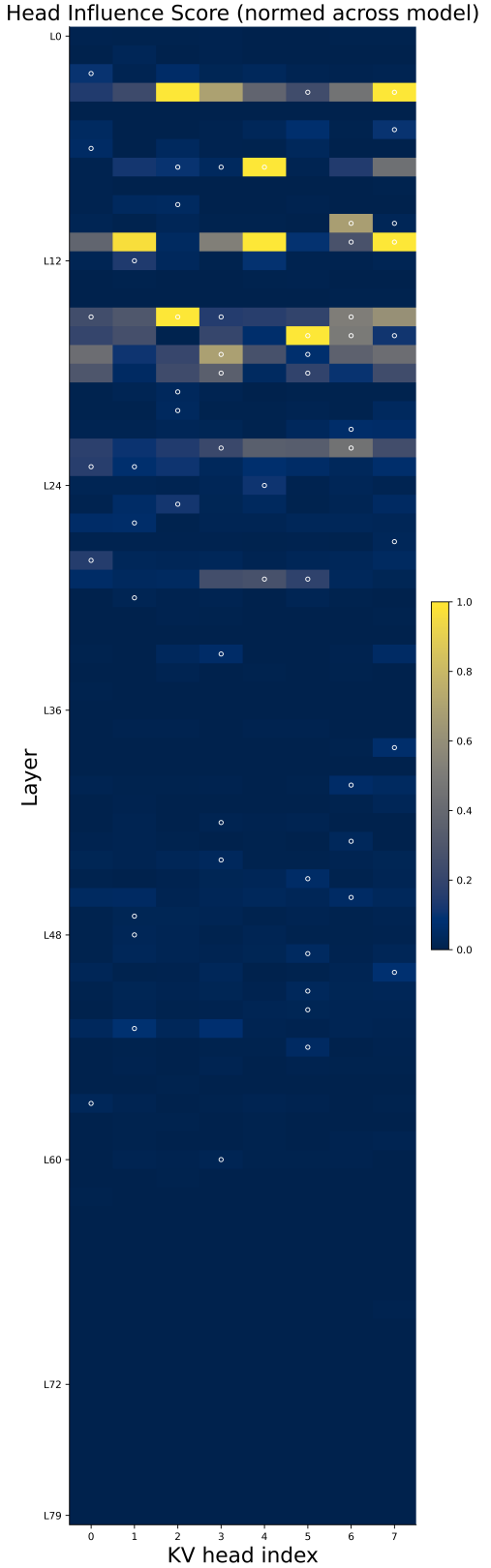


Figure 7. Head selection for Qwen2.5-VL-72B under a input-text:image token ratio of 1:2.

Table 9. **Trainable parameters (M) and per-example FLOPs (G) - Qwen2.5-VL-7B.** We test on ScreenSpot-Pro across input-text:image token ratios for the Qwen2.5-VL-7B model. Image-LoRA is V-only configurations.

Text:Img Token Ratio Avg #Image Tokens	1:5 4195		1:4 3367		1:3 2534		1:2 1677	
	Params (M)	FLOPs (G)	Params (M)	FLOPs (G)	Params (M)	FLOPs (G)	Params (M)	FLOPs (G)
Image-LoRA	0.6298	15.85	0.6298	12.72	0.6298	9.576	0.6298	6.335
Std-LoRA V-only	0.9175	27.83	0.9175	23.27	0.9175	18.68	0.9175	13.96
Std-LoRA QV	2.523	76.53	2.523	63.99	2.523	51.38	2.523	38.38
Std-LoRA QKVO	5.046	153.1	5.046	128.0	5.046	102.8	5.046	76.76

Table 10. **Trainable parameters (M) and per-example FLOPs (G) - Qwen2.5-VL-72B.** We test on ScreenSpot-Pro across input-text:image token ratios for the Qwen2.5-VL-72B model. Image-LoRA is V-only configurations.

Text:Img Token Ratio Avg #Image Tokens	1:5 4195		1:4 3367		1:3 2534		1:2 1677	
	Params (M)	FLOPs (G)	Params (M)	FLOPs (G)	Params (M)	FLOPs (G)	Params (M)	FLOPs (G)
Image-LoRA	3.012	75.80	2.945	59.49	2.881	43.80	2.877	28.94
Std-LoRA V-only	5.898	178.9	5.898	149.6	5.898	120.1	5.898	89.72
Std-LoRA QV	16.38	496.9	16.38	415.5	16.38	333.7	16.38	249.2
Std-LoRA QKVO	32.77	993.9	32.77	831.0	32.77	667.3	32.77	498.4

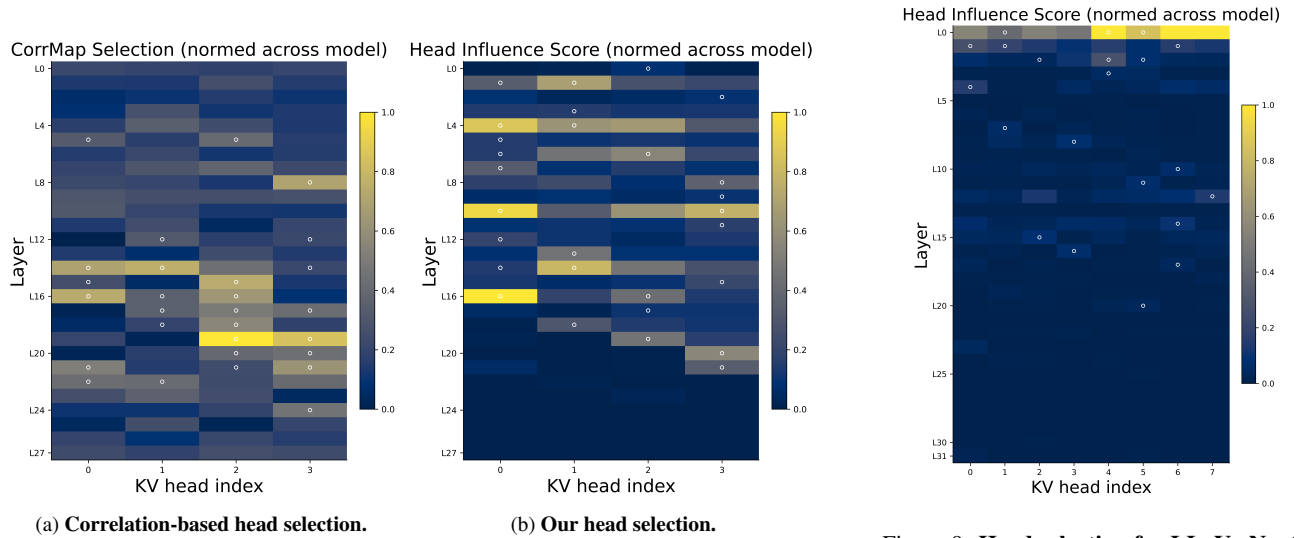


Figure 8. **Comparison between the correlation-map-based approach and our proposed head-selection method.**

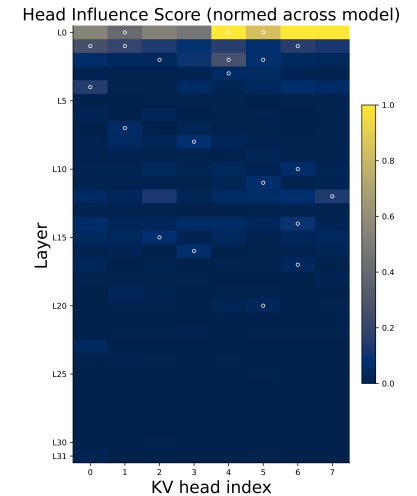


Figure 9. **Head selection for LLaVa-Next-7B under 1:2 text:image ratio.**

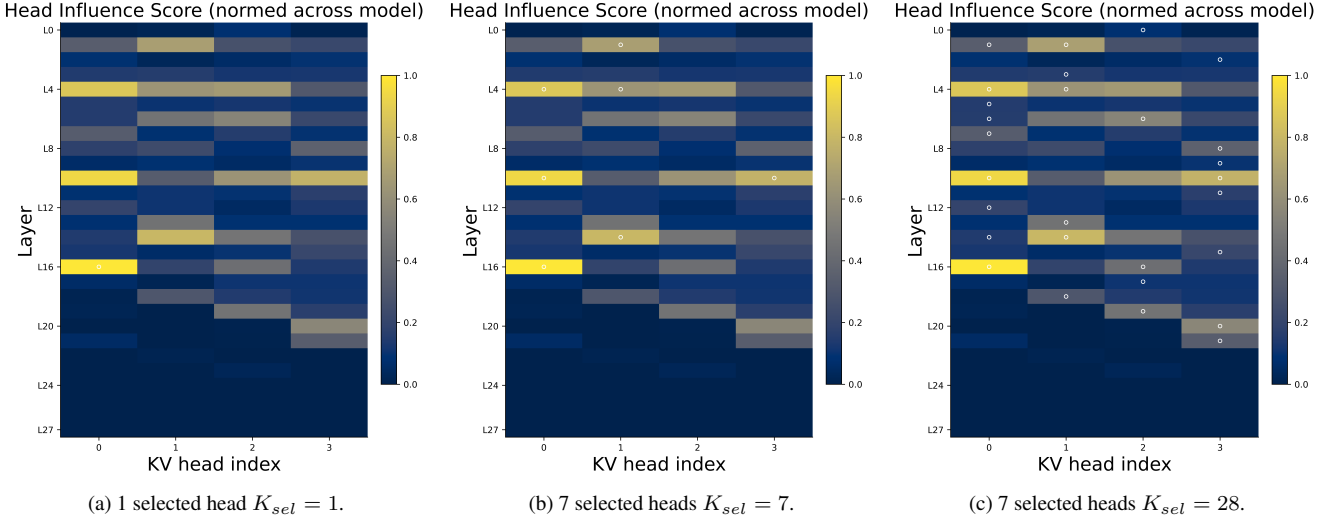


Figure 10. **Head selection patterns under different head budgets.** The head selection procedure uses default hyper-parameters of  $\tau = 0.5$  and  $\rho = 2$ . All results are obtained on ScreenSpot-Pro using the 1:2 input-text:image token ratio.

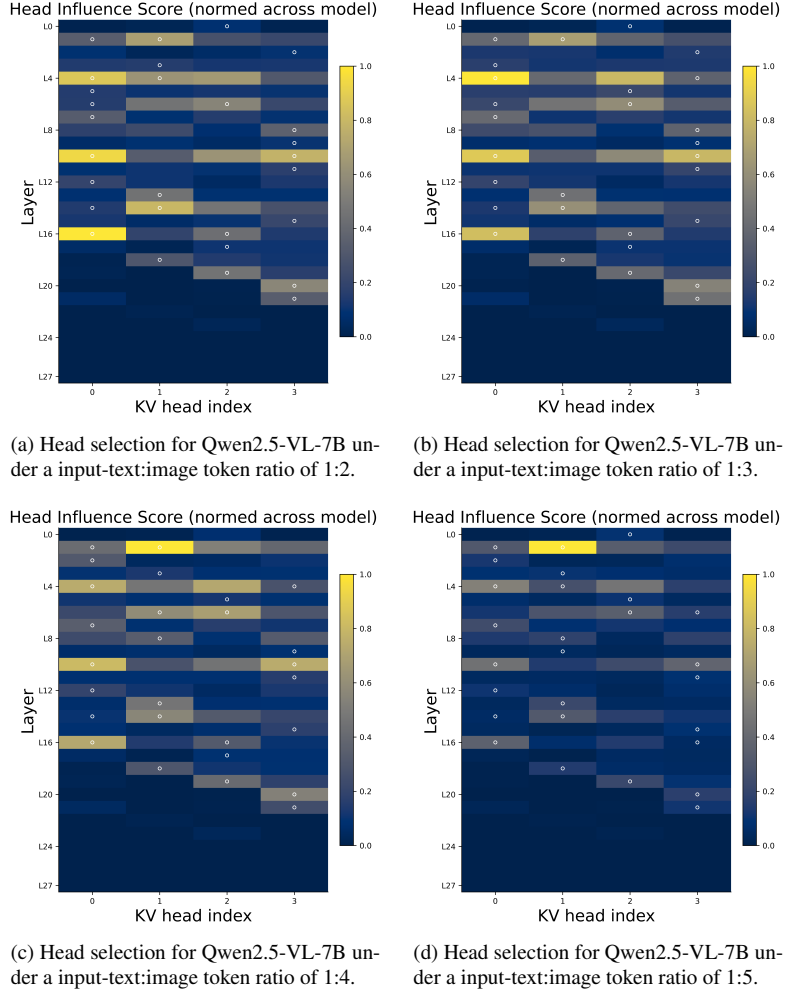


Figure 11. **Head selection for Qwen2.5-VL-7B across different input-text:image token ratios on ScreenSpot-Pro.** Although ratios (and thus image resolutions) differ, the resulting head selections remain similar, with minor variations.